# Boundaries of Acceptable Defectiveness: Redefining Surface Code Robustness under Heterogeneous Noise

Jacob S. Palmer

Computer Science

Northwestern University

Evanston, U.S.A.

JacobPalmer2026@u.northwestern.edu

Corresponding Author

Kaitlin N. Smith
Computer Science
Northwestern University
Evanston, U.S.A.
kns@northwestern.edu

Abstract—A variety of past research on superconducting qubits shows that these devices exhibit considerable variation and thus cannot be accurately depicted by a uniform noise model. To combat this often unrealistic picture of homogeneous noise in quantum processors during runtime, our work aims to define the boundaries of acceptable defectiveness (BADs), or the upper boundary of a qubit's physical error, past which this defective qubit entirely degrades the logical computation and should be considered faulty and removed from the surface code mapping. Using the QEC simulation package STIM, repetition code circuits on rotated surface codes were generated, sampled, and analyzed from distances 3 to 17, with various defective error rates and outlier defect locations (i.e., a measurement / data qubit with high error in the center of the lattice). In addition, we simulated heterogeneous noise models using the same parameters to test how increasingly deviated distributions of physical errors scale across code distances under realistic, heterogeneous noise models that are informed by current superconducting hardware. The results suggest that there are, in fact, boundaries of acceptable defectiveness in which a defective qubit, with a physical error rate >75%, can be left in the lattice with negligible impact on logical error rate given sufficient code distances and proper placement in the lattice. On the other hand, we find that substantial qubit variation around a seemingly acceptable physical error rate can severely degrade logical qubit performance. As a result, we propose that defectiveness of both individual qubits and the overall uniformity of lattice fidelity should not be viewed as all or nothing, but instead as a spectrum. Our research demonstrates how heterogeneity directly impacts logical error rate and provides preliminary goals and metrics for hardware designers to meet in order to achieve target logical performance with imperfect, non-uniform qubit qualities.

#### I. Introduction

Quantum error correction (QEC) enables fault-tolerant quantum computing by utilizing multiple physical qubits to redundantly encode a single abstract logical qubit, thereby making the information more resilient to errors such as decoherence or gate noise [8]. A leading method for QEC is the surface code (SC), in which physical qubits are arranged in a 2D lattice, and operations are performed between neighboring qubits [9]. The SC is favorable for near-term QEC demonstrations because of its high noise tolerance, and defective qubits in the 2D lattice can be managed by deforming the

lattice around the defect at the cost of additional physical qubit overhead [2, 25]. Existing SC research explores (1) how logical error rate (LER) is affected by physical error rate and (2) how physical overheads are impacted by defects. However, analysis often considers physical qubit performance, specifically in regard to superconducting qubit architectures, in a rigid, homogeneous manner wherein physical qubits are either characterized as either uniform in their error rates or completely unusable. As a result, critical insights into the impact and upper bounds of the usability of qubits that range in their defectiveness are currently sparse. A better understanding about how SC tolerates heterogeneous error landscapes is necessary to improve the mapping of QEC to realistic quantum systems.

The primary goal of this work is to more clearly understand how the SC responds whenever physical error rate more closely resembles a distribution rather than a constant value. Using the QEC simulation package STIM, we investigate the impacts of defective outlier qubits as well as heterogeneous noise on overall LER on code distances ranging from 3 to 17. Our contributions are as follows:

- We model the performance of surface code under heterogeneous noise models, providing novel insights into how logical performance on non-perfect quantum devices scales with increasingly deviated physical noise distributions
- For the first time, we define the concept of boundaries of acceptable defectiveness (BADs) as a way to examine and quantify the performance and thresholds for imperfect noise models. The community lacks quantitative guidance with respect to the question of "how defective is too defective" for qubit error distance from the mean. Our research shows the utility of considering physical error rate as a distribution when picking the best SC solution to achieve an algorithm's target logical error. Further, our simulation results show (1) the existence of BADs in both homogeneous and heterogeneous noise models and (2) these BADs are not static and differ greatly depending on

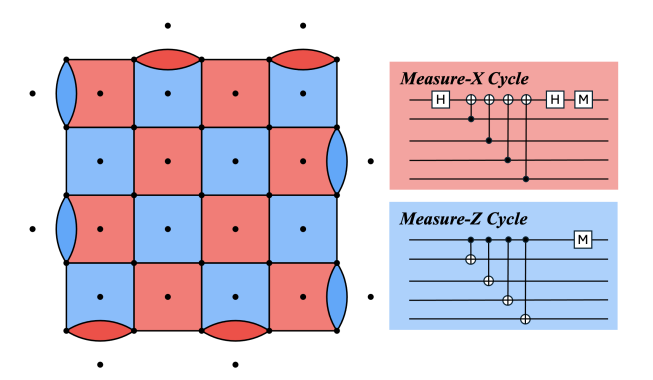


Fig. 1. An example visualization of a d=5 rotated surface code lattice (left) where data qubits are found on the grid boundaries, and X (Z) measurement/stabilizer qubits are found within the red (blue) squares of the grid. The sequence of operations (right) for a single Measure-X and Measure-Z surface code cycle are also illustrated.

the assumed noise model (i.e., the quality of qubits within a lattice) and targets for LER. Real quantum hardware exhibit vast variation in noise and thus in the pursuit of grounding our simulated models in reality, identifying the BADs allows a more accurate understanding of how performance scales given any arbitrary noise model.

• We developed a novel circuit generator framework using STIM for rapid experimentation of SC performance under any arbitrary and unique noise model. Our code, which will be open-source, creates quantum circuits with complete granular control of each individual qubit's fidelity, enabling comparison across any configuration of noise models. It also provides novel generation of heterogeneous noise models based on deviations from a mean physical error rate. This tool has a high potential to find utility in QEC resource estimation and design space exploration based on superconducting qubits. This code and demo notebooks used to generate the figures within this paper can be found here on GitHub

#### II. BACKGROUND

#### A. The Surface Code

The surface code [8] (SC) is one of the most promising QEC codes for physical realization, especially with superconducting qubits, due to its implementation using a 2D nearest-neighbor qubit layout, and its high tolerance to noise [8]. Recent demonstrations on superconducting circuits have allowed logical qubits to be demonstrated and LERs to drop below threshold [22]. SCs can implement a universal set of gates, create logical entanglement with lattice surgery [16], and generate magic resource states with magic state distillation [17, 12]. In this work, we focus on the rotated SC (i.e. any further mention of SC is assumed to be this), requiring  $2d^2 - 1$  physical qubits per logical qubit. Our goal is study the surface code's ability to store logical qubit states over time while being subject to various noise models.

An illustration of a d=5 SC patch can be seen on the left side of Fig. 1. In this picture,  $d^2$  data qubits are found on the

edges of the grid while  $d^2-1$  measurement qubits are found within the red and blue squares representing Measure-X and Measure-Z stabilizers, respectively. The right side of Fig. 1 shows the sequence of operations performed during the surface code cycle that allows the data qubits (bottom four lines) to interact with the measurement qubit (top line). Over many cycles, the history of detection events gives insight to the errors happening during runtime. These syndromes are then used by the decoding algorithm, minimum-weight perfect matching [6] in our case, to locate the error within the logical qubit so that it can be corrected. A logical error is introduced into the surface code when at least d/2 errors occur along a non-trivial path.

#### B. Previous Work

The heterogeneous nature of superconducting qubit physical qubit error has been well-documented [20, 27, 4]. Prior work has proposed novel architectures, such as those based on chiplets [24], to promote device scaling with more uniform metrics, but it is unlikely that quantum systems comprised of imperfectly fabricated processors will ever demonstrate perfectly heterogeneous noise. This raises many challenges in terms of how to design QEC strategies that best meet the needs of algorithms while managing realistic constraints of hardware.

Previous work with the SC has made progress in combating the reality of defective qubits by leveraging "super stabilizers" or boundary deformations in the SC patch. These techniques work by routing the stabilizer measurement circuits so that they avoid faulty components [15, 5, 29]. Current deformation methodologies incur a tradeoff: deform the lattice around the defect, thus, removing the defect's negative impact on the LER *but* incur additional resource overhead in the process. This increase in overhead is typically a higher physical qubit requirement, but some deformation techniques also incur increased complexity during compilation or runtime as a result of specialized steps to facilitate computation within the deformed lattice.

Most work in SC defect management assumes a rigid categorization of qubit quality in the sense that a qubit is either operating at the mean physical error rate or it is completely unusable and should be dropped out of the logical qubit mapping. However, more lenient bounds of acceptable defectiveness could exist, especially in the case where the distribution of physical qubit error rates are characterized by a standard deviation. For example, the work in [19] reports that the current variation in coherence time seen on existing superconducting qubits leads to hindered LER with the SC. This presents the question of how defects should be defined, and which qubits with higher error rates can be left in the lattice in its current state, given the QEC designer's choice of code distances. These sorts of estimates remain to be fully explored; as such, this work serves as a starting point for scaffolding out potential defects, their impacts, and the design choices necessary to minimize detrimental effects. To narrow or scope in this initial exploration of defining BADs, we focus on distributions associated physical qubit error (Section II).

# III. HOMOGENEOUS VS. HETEROGENEOUS ASSUMPTIONS OF NOISE ON SURFACE CODE LATTICES

In general, if physical operations on the SC are performed below a sufficiently low critical noise threshold then logical error rates are exponentially suppressed with increasing code distances [9]. This scaling can be expressed by the relation:

$$\varepsilon \propto \left(\frac{p}{p_{thr}}\right)^{\frac{d+1}{2}}$$

where  $\varepsilon$  is LER,  $p_{thr}$  is some threshold for physical noise tolerance, and d is the distance of our code [1]. Prior work has found  $p_{thr}=0.0057$  [9]. In this general form relation, p represents the physical error rate of all  $2d^2-1$  physical qubits that encode our singular logical qubit in a given lattice. Thus, this relation assumes a uniform, homogeneous physical noise exhibited across the lattice. However, results from real quantum devices have shown that superconducting quantum devices do not exhibit a uniform noise over the entire processor but instead vary greatly in qubit fidelity.

#### IV. SIMULATION FRAMEWORK OVERVIEW

The simulation and analysis framework we devised generates and samples the performance of parameterized repetition code circuits on rotated surface codes using Python and STIM [11]. The generated circuits consists of a 2D lattice with  $n=2d^2-1$  qubits scaled from a provided distance d. STIM is specifically designed for rapid design and simulation of quantum stabilizer circuits, and our code was built using the STIM Python package [10]. While other popular quantum circuit simulators exist [13, 7] STIM was selected for 1.) the ability to adaptively create entire stabilizer circuits from string manipulation and 2.) it offers very fast runtime allowing for sampling millions the logical error count from millions of shots in minutes. For example, in our distributed heterogeneous noise simulations in Section V-C, the simulations (Fig. 11 and Fig. 12) consist of nearly  $4 * 10^8$  total shots over the 8 distances sampled for each, with each point representing a generated circuit with a unique noise distribution run approximately  $5 * 10^6$  times. Thus, it was important that the simulation tool be reasonably fast in order to test a wide variety of different input parameters when developing our code and analyzing our results.

The circuits are generated with a variety of input parameters to facilitate testing variations in both individual qubit noise (e.g., specific defect location and defect physical error rates) and overall lattice noise distributions (e.g., uniform or heterogeneous). Our code works in three parts (1) generating the parametrized STIM string representation of the measurement circuit, (2) parsing the simulation data and performance results provided by STIM into usable DataFrames, and (3) directly plotting simulation data into easy-to-understand plots that allow for immediate comparison of performance across any number of code distances. Each of these circuits is built using either a uniform (homogeneous) or normally distributed (heterogeneous) noise distribution. For circuits built with a

homogeneous noise model, all qubits within the lattice will be assigned the same physical error rate p value is given as a parameter and used as the error rate for all qubits in the lattice. For this initial foray into heterogeneous noise models, we are assuming a simplified notion of noise. Specifically, our simulation primarily uses depolarizing channel (D) noise is a standard quantum noise model in which a qubit becomes depolarized with a given probability p [28]. In most conversations, p is referred to as the level of noise of a physical qubit, including more types than just depolarization noise [9]. However, in this simplified noise model, we rely solely on noise occurring as a result of Pauli-X (bit-flips) errors on state preparation and measurement and depolarization error on gate operations to introduce noise. In reality, quantum noise can be introduced by a wide variety of sources, such as interactions with the environment, uncontrolled interactions with other qubits, imperfect operations, or leakage [23]. Additionally, noise can be introduced permanently on specific qubits as a result of manufacturing defects on the superconducting devices [3]. Implementing a more complex noise space is an area that could be greatly extended upon and is discussed further in our future works section.

#### A. Building circuits as STIM strings

For a given distance d, the generators first assign each of the  $n=2d^2-1$  qubits a coordinate pair (X, Y) within a grid representing the 2D lattice. The set of values for both the x-coordinate and the y-coordinate starts at 0.5, increments by 0.5, and goes up to (d+0.5).

In SCs, each qubit is either a measurement (stabilizer) qubit or a data qubit [9]. Within our generators, data qubits are always located at integer coordinates (i.e. (3, 5)) and measurement qubits are always located at non-integer coordinates  $\pm .5$  in x or y direction from the data qubits (i.e. (.5, .5)) or (1.5, 2.5)). Within our setup, data qubit coordinates are always integer values, while the measure qubits will always be  $\pm .5$  from their respective data qubits.

Because STIM strings represent the stabilizer circuits in a manner similar to quantum circuit diagrams [21], each of the n qubits is referred to by a wire index from 0 to n-1. Our generators map coordinate pairs to the appropriate wire index within the STIM string, allowing for the generators to accept coordinates as inputs for specific noise models and then appropriately translate between the index and coordinate references for any given qubit. Additionally, the generators will map special location keywords to coordinates on the lattice, as seen in Fig. 2. Since the distance directly determines the grid space, these special keywords facilitate placing defects at the same relative location in the lattice, simplifying cross-distance performance analysis.

There are two primary generator types, which assume what type of noise distribution the lattice displays:

1) Homogeneous Distributions: The homogeneous generator takes as input a physical error rate p that will be set as the standard physical error rate for all qubits in the lattice.

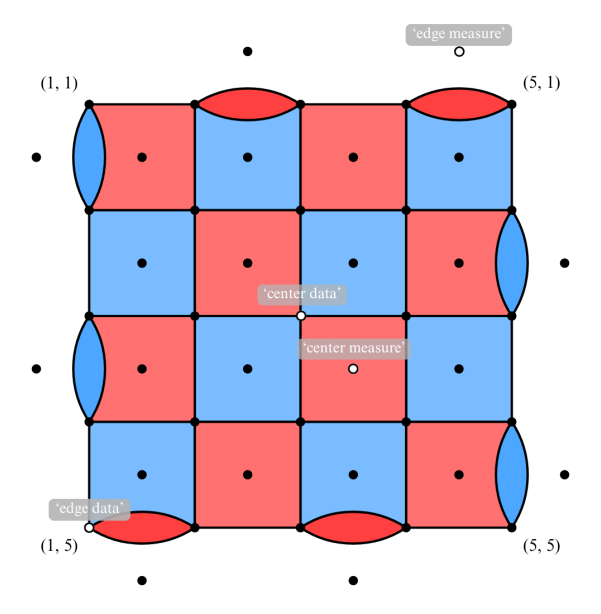


Fig. 2. For the simulations and selection of defect locations, the generators optionally allow for specific qubit locations to be designated in order to maintain similarity across various code distances. The qubit locations are marked by the special case strings, 'center data', 'center measure', 'edge data', 'edge measure'. These special case strings are then converted by calculating their respective coordinate given any lattice of distance d.

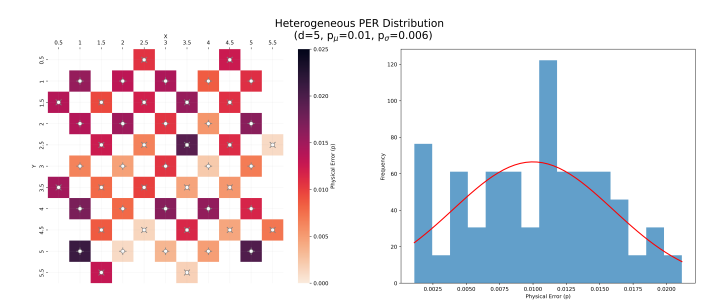


Fig. 3. A heatmap and distribution representing a randomly distributed heterogeneous noise distribution on a d=5 code. The distribution on the left is shown to demonstrate that, although the truncated normal distribution results in slight differences, the samples still form a distribution around  $p_{\mu}$  and  $p_{\sigma}$ . Within all heatmaps shown, data qubits are denoted by + and measurement qubits are denoted with X.

2) Heterogeneous Distributions: As discussed earlier, a primary motivation for this research is to provide methods for exploring and analyzing simulation models that more accurately resemble real superconducting devices [18, 1]. To achieve this, the heterogeneous generator creates a circuit that models the performance of a non-perfect lattice with individual qubits' physical error rate spanning a distribution of noise values, rather than a static p. Each qubit's physical error rate is randomly pulled from a truncated random normal distribution created based on two input parameters: a mean physical error rate,  $p_{\mu}$ , and a standard deviation,  $p_{\sigma}$ . Each time a circuit is generated, a new random distribution will be sampled from, creating an entirely unique distribution of heterogeneous noise between circuit generations (even with identical parameters),

as seen in Fig. 3 for a d=5 code. This unique distribution for each generated circuit is, in part, a modest reflection of how the noise exhibited by superconducting qubits can greatly fluctuate during or between runtime, but introduces some variability in our simulation's performance results that leads to some trends being non-monotonic, something that is discussed in Section V later on.

It is important to note that noise distribution on current superconducting devices does not necessarily follow a Gaussian model [26]. However, within our simplified model of noise, it is reasonable to assume that, while not fully reflective of the noise model of today's quantum devices, it is more practical and aligned with realistic error landscapes than a uniform model. Additionally, as quantum processors increase in capacity, it is also reasonable to assume that distributions will begin to converge to a normal distribution, given the central limit theorem. Thus, as a preliminary method for distributing noise in a lattice, this normal distribution is sufficient, and our parameterized modeling allows for other distributions to be explored.

In our experiments, we use this heterogeneous generator to examine the performance over a wide range of  $p_{\mu}$  and  $p_{\sigma}$  values. Portions of this range are either well past accepted physical threshold values or far below the physical noise capabilities of current quantum devices. However, sampling over this large range, even if some values are impractical, is intended to examine overall trends in heterogeneous models and thus is a critical component of our initial aim for this project.

### B. Defective Qubits

Both homogeneous and heterogeneous circuit generators accept a number of parameters, including distance, rounds, maximum shots. More importantly, the generator methods allow individual defect(s) to be arbitrarily created at any part in the lattice by providing a qubits coordinate (x, y) pair within the lattice (as seen in Fig. 2) and a physical error rate for each defect,  $p_{def}$ . In practice, the generators could be used to manually set the physical error rate for each qubit in the lattice simultaneously, providing complete granular control over the simulated noise.

#### C. Operational Noise

In the generators, noise is introduced right before circuit elements (e.g., gates and measurements) as a noise operator with the general format for 1q operations:

<1q noise type> <qi index> <pval\_qi>
and for 2q operations:

Each qubit is assigned an individual error rate,  $p_i$ , where i is the index of the qubit.  $p_i$  determines the error rate for all operation involving this qubit. These operations include all multi-qubit operations ("DEPOLARIZE2"), single-qubit operations ("DEPOLARIZE1"), and measurements ("X-ERROR")

on the qubit. The  $p_i$  is scaled based on single or two-qubit operations. Generally, multi-qubit operations are more prone to errors than operations involving only a single qubit. Thus, it should be reflected that CX operations involving the defective qubits would exhibit a higher error rate than their single-qubit operations. Thus, for two-qubit depolarization noise associated with CX operations, the error rate is set as a mean of the  $p_i$  corresponding to the two qubits involved in the operation. Since two-qubit operations are more prone to error than single-qubit operations [1, 18], two-qubit noise has an additional scaling factor, s, on the  $q_i + q_i$  mean, in the form:

$$p_{CX} = \left(\frac{p_{q1} + p_{q2}}{2}\right) * s$$

This scaling factor is set as s=1.2, representing a 20% increase over single qubit operations. For single-qubit depolarization and Pauli-X, the value for each operation on a qubit  $q_i$  is set directly to its corresponding  $p_i$  value.

#### V. CASE STUDIES AND ANALYSIS

To demonstrate the performance disparity between heterogeneous and homogeneous noise assumptions, we examined how LER scales across code distances 3-17 when assuming a homogeneous vs. heterogeneous noise model. In each case, the logical error rate per round,  $\varepsilon$ , is the metric used to evaluate performance. Every measurement circuit generated for these experiments contains 3 rounds, and the logical error rate is considered as the average number of errors that occur per round in the measurement circuit:

$$\varepsilon_{round} = \left(\frac{errors}{shots*rounds}\right)$$

To facilitate comparison and benchmarking across the four cases, we establish a target logical threshold,  $\varepsilon_{thr}$ , of 0.0057 based on the work of [9]. The target logical threshold to use as a baseline depends largely on the fidelity required to support a specific algorithm or application on a particular quantum device. However, for our purposes, we assume that a  $\varepsilon_{thr}=0.0057$  is assumed to be sufficient fidelity for these memory experiments. For each case, a heatmap was generated to visually represent an approximate noise distribution on a d=5 rotated surface code lattice. This

In our experiments, four primary cases were selected under increasingly complex models of noise: (1) a completely uniform homogeneous lattice, (2) a uniform homogeneous lattice with a singular defect in the center data qubit, (3) a heterogeneous lattice, and (4) a heterogeneous lattice with a singular defect in the center data qubit. In each case, the simulations increase in complexity of the noise models, allowing differences in performance scaling with distance to become evident.

In these experiments, we once again return to the idea of the "boundary of acceptable defectiveness", or BADs. For each code distance, the boundary of acceptable defectiveness (BAD) defines the maximum physical noise tolerance after which the LER surpasses our target logical threshold. Within the figures for each of our case experiments, the BAD for each code distance is precisely at the intersection point between the target logical threshold and the distance's performance curve. Once the physical noise level has surpassed the BAD, we can consider the lattice to be effectively too noisy and the computation unusable.

#### A. Case 1: Homogeneous Noise

For the first scenario, Case 1 covers the assumption of uniform noise in which all physical qubits within a lattice unilaterally express the same p noise. A heatmap for this uniform homogeneous noise model can be seen in Fig. 4. The performance results for Case 1 are shown in Fig. 5 for d=[3, 5, 7, 9, 11, 13, 15, 17]. In past literature, this most

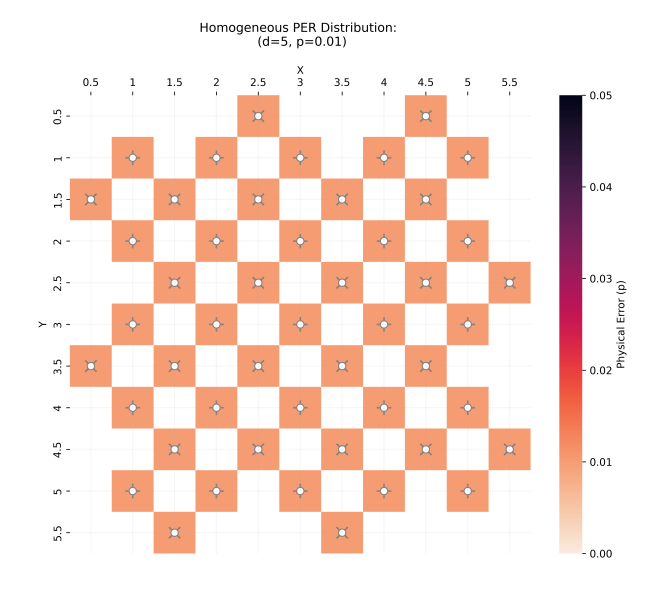


Fig. 4. (Case Study 1) Heatmap for a homogeneous noise model on a d=5 code with no defects or deviations. In this heatmap, data qubits are denoted by + and measurement qubits are denoted with X.

closely resembles the ideal and common notion of how noise is represented in SC. As shown in Fig. 5, all distances (with the exception of d=3) cross the  $\varepsilon_{thr}$ . For the highest distance sampled, d=17, the BAD is at  $p \approx 0.00614$ . Any d=17 lattice with a p < 0.00614 would, in this theoretical model, be sufficient for computation. However, if our goal is to minimize the code distance and thus our physical qubit overhead, we would select the minimum viable code distance for which our device's expressed p is below the distance's respective BAD. In this uniform homogeneous model, the d=5 code has a BAD at approximately  $p \approx 0.003$ . Thus, if deciding an optimal code distance for a physical device capable of performing computation with physical noise,  $p \approx 0.003$ , we should select the d=5 code. While achieving p = 0.003 on a real superconducting device might be out of reach with current hardware [14], analyzing the BADs for a given code distance with a realistic physical noise model allows for additional optimization considerations. A completely uniform noise model is ideal, with performance requirements met at all but the smallest distance, d=3. While achieving uniform

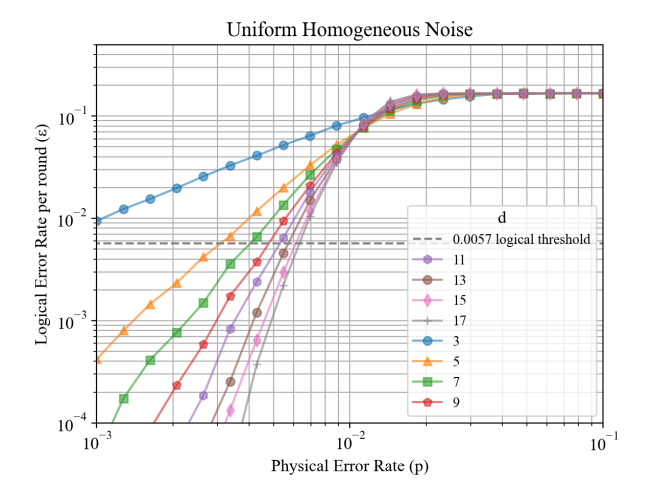


Fig. 5. (Case Study 1) Performance results for a completely uniform, homogeneous noise model across distances d=[3, 5, 7, 9, 11, 13, 15, 17]. Case 1 represents the most ideal noise model assumptions when considering surface codes in that all qubits within the lattice have an identical quality of p and no qubit deviates from this value. In Cases 2 and 3, the blue line in each performance result figure is the baseline for each distance when no deviation is expected. As such, each line in this figure is identical to the blue baseline in the Case 2 and Case 3 performance results for the corresponding distance.

noise across all physical qubits results in the highest overall fidelity and the most viable code distances, noise data from superconducting devices exhibit significant variations in noise within a given chip. Thus, this uniform model, at least for superconducting devices, is naive and an unrealistic basis for accurately modeling SC robustness [14, 18].

#### B. Case 2: Homogeneous Noise with Outlier Defects

To test individual qubit impact within a homogeneous noise model, two separate circuits were generated with a defect located at the center data qubit and near-center measure qubits. In this second scenario, we examine the impact of a singular defect on the surface code's performance under an otherwise uniform noise model. A heatmap for the homogeneous noise model with outlier defect center data qubit can be seen in Fig. 6. The performance results for Case 2 are shown in Fig. 7 for d=[3, 5, 7, 9] and Fig. 8 for d=[11, 13, 15, 17].

In this experiment, all lattices across the sampled distances have a defect located at the data qubit in the center of the lattice. We simulated the performance with the defect center data qubit  $p_{def}$  value ranging from 0.05 to 0.75. At the upper end of the  $p_{def}$  values sampled, the individual qubit is essentially completely unreliable, with roughly 75% of operations on this qubit resulting in an erroneous computation. The results of this experiment (Fig. 7, Fig. 8, and Fig. 9) show an incredibly strong resilience to the individual defect. Similar to that of the unilateral homogeneous model in Case 1 (Fig. 5), all but the smallest code distance d=3 (Fig. 7) were able to meet our target logical threshold. In the worst case with  $p_{def}$ = 0.75, the BAD for the d=17 code (Fig. 8) is  $p \approx 0.005981$ . In comparing this to the d=17 performance in Case 1 (Fig. 5), the maximally defective qubit only reduced our BAD by 3%.

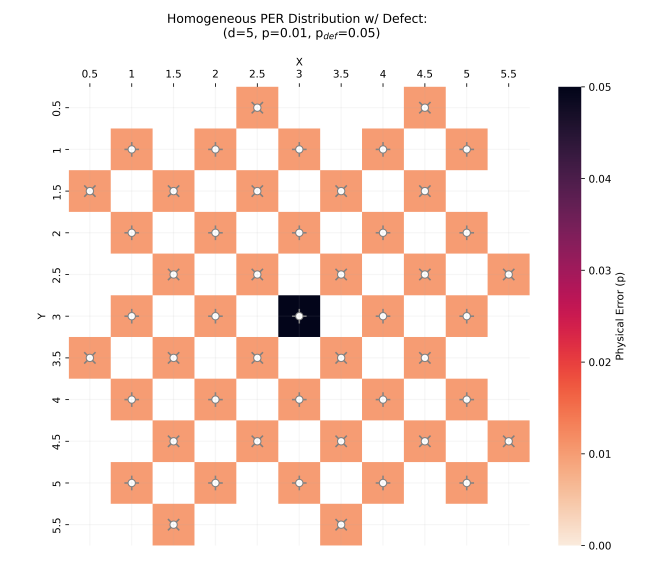


Fig. 6. (Case Study 2) Heatmap for a homogeneous noise model on a d=5 code with a defect on the center data qubit. The  $p_{def}$  shown in this heatmap is 0.05 to show this distribution, but significantly higher values  $p_{def}$  are also used in the Case 2 experiments as well. In this heatmap, data qubits are denoted by + and measurement qubits are denoted with X.

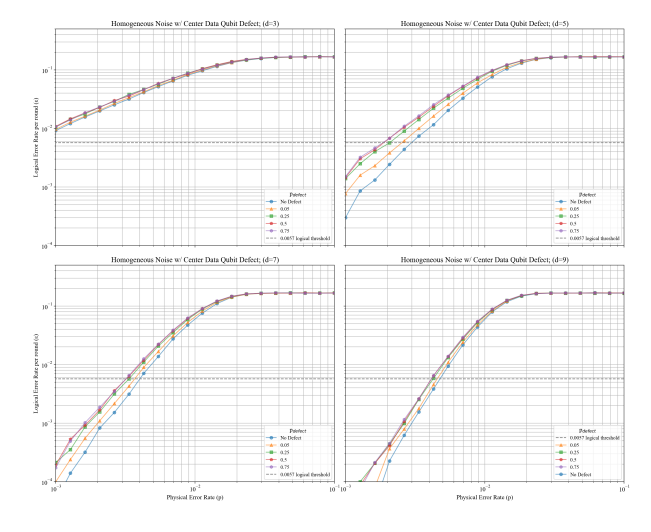


Fig. 7. (Case Study 2) Performance of homogeneous noise model with outlier center data defect over d=3 through d=9.

For the minimum viable code distance in Case 2, d=5 (Fig. 7), the BAD is located at  $p\approx 0.001842$ . In comparing the BAD for d=5 in Case 2 with the BAD for d=5 ( $p\approx 0.003$ ) in Case 1 (Fig. 5), the presence of the defect with  $p_{def}=0.75$  resulted in a larger reduction to our acceptable boundary by about 63%. As with physical noise tolerance, the results here suggest that under a homogeneous noise model, an increase in code distance also directly results in a significant increase in the resilience to individual defects with high levels of noise.

#### C. Case 3: Heterogeneous Noise

In the third scenario, we expand our noise model to a heterogeneous distribution of physical errors and examine the

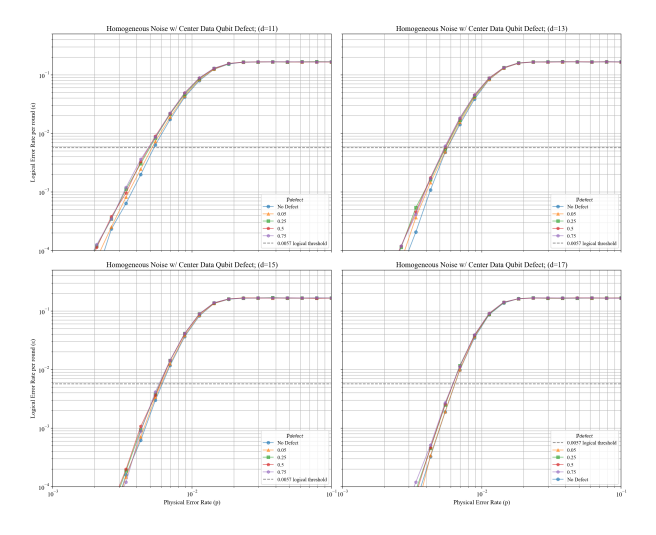


Fig. 8. (Case Study 2) Performance of homogeneous noise model with outlier center data defect d=11 through d=17.

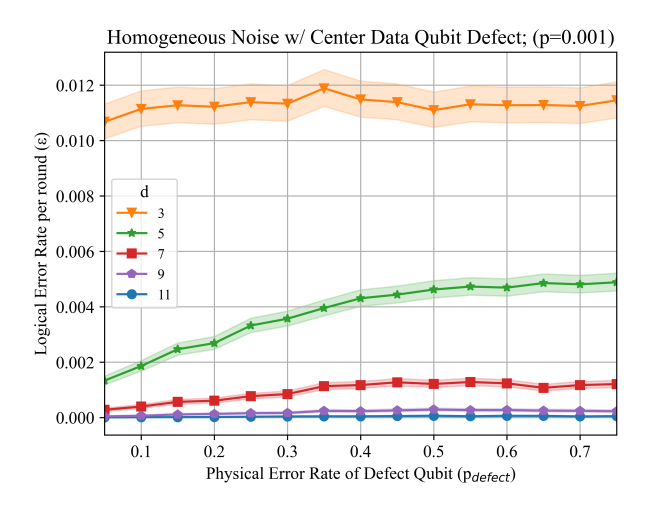


Fig. 9. (Case Study 2) Logical error rate vs. defective physical qubit error rate for code distances d=[3, 5, 7, 9, 11]. To further examine how performance is affected across code distances, this figure shows a similar homogeneous noise model to that in Case 2, except that the noise for all other qubits is kept constant at p=0.001. As we increase our code distance, the lattice becomes increasingly resilient to the noise introduced by the defective data qubit, as expected. At distances of 9 or above, the performance is essentially unaffected by the presence of the defective qubit. Thus, this further suggests that the impact of highly defective qubits becomes negligible at a sufficiently large code distance.

impact on the logical performance. A heatmap demonstrating a potential configuration for a d=5 heterogeneous noise model can be seen in Fig. 10. The performance results for Case 3 are shown in Fig. 11 for d=[3, 5, 7, 9] and Fig. 12 for d=[11, 13, 15, 17]. For this experiment, we simulate heterogeneity by assigning each circuit a uniquely generated noise distribution. On each circuit, each qubits p is randomly sampled from a truncated normal distribution with a mean noise value,  $p_{\mu}$ , and a noise deviation,  $p_{\sigma}$ . To examine the impact of this heterogeneous noise on logical performance, we simulated 5  $p_{\sigma}$  values ranging from 0.006 to 0.015. Similar to Case 1 (Fig. 5) and 2 (Fig. 7 and Fig. 8), the performance of

the heterogeneous noise is benchmarked against a uniform homogeneous distribution, which is equivalent to when the  $p_{\sigma}$ = 0.0. The non-monotonic behavior of the plotted data in Fig. 11 and Fig. 12 is a result of this randomly sampled distribution, in which some circuits have a higher distribution of physical noise placed on more detrimental locations, such as measurement qubits or edge qubits of which noise present has a greater impact on LER [8]. However, the noise and coherence properties of individual superconducting qubits can change frequently [14]. Thus, purely monotonic performance curves when utilizing superconducting qubits is not a guarantee.

In Case 3, there are significant deviations from the trends examined in Case 1 and Case 2 with homogeneous noise models. Under the heterogeneous model, the minimum viable code distance is at d=9 (Fig. 11) or d=11 (Fig. 12) in this heterogeneous model, as opposed to the minimum viable code distance at d=5 for both the uniform homogeneous (Fig. 5) and singular defect homogeneous models (Fig. 7). For d=9 (Fig. 11) in Case 3, only one intersection with the target logical threshold occurs at  $p_{\mu} \approx 0.0018$  when the noise deviation is relatively low at  $p_{\sigma} = 0.006$ . With no deviation ( $p_{\sigma} = 0.0$ ) at d=9, the intersection with the target logical threshold occurs at  $p_{\sigma} \approx 0.00466$ . In the presence of heterogeneous noise, the BAD is reduced by approximately 90% at the minimum viable code distance, d=9.

#### D. Case 4: Heterogeneous Noise with Outlier Defects

In the fourth scenario, we examine performance changes under a heterogeneous noise model in the presence of a center data-defect qubit. A heatmap demonstrating a potential configuration for a d=5 heterogeneous noise model with a center defect can be seen in Fig. 13. The performance results for Case 3 are shown in Fig. 14 for d=[3, 5, 7, 9] and Fig. 15 for d=[11, 13, 15, 17]. The location of the defect (center

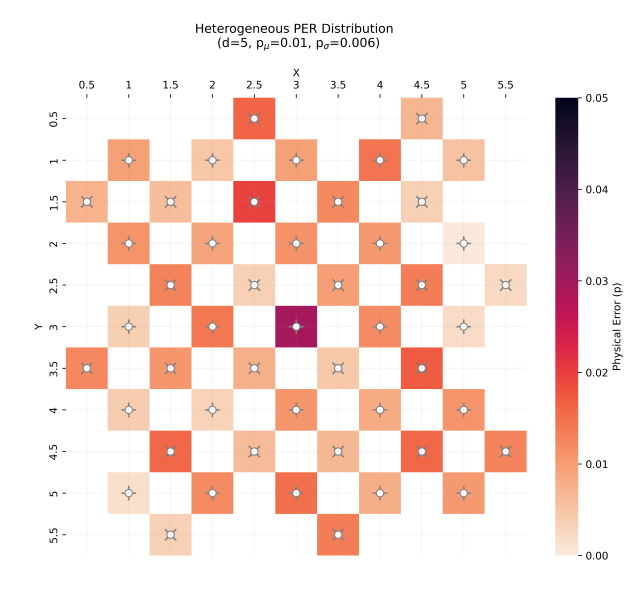


Fig. 10. (Case Study 3) Heatmap for a heterogeneous noise model on a d=5 code. Data qubits are denoted by + and measurement qubits are denoted with **X**.

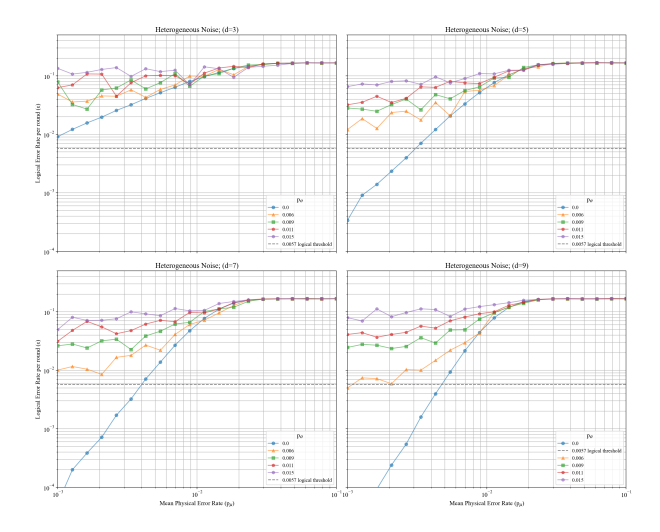


Fig. 11. (Case Study 3) Performance of heterogeneous noise model for distances 3 through 9. The blue line  $(p_{\sigma}=0)$  represents a unilateral homogeneous noise model.

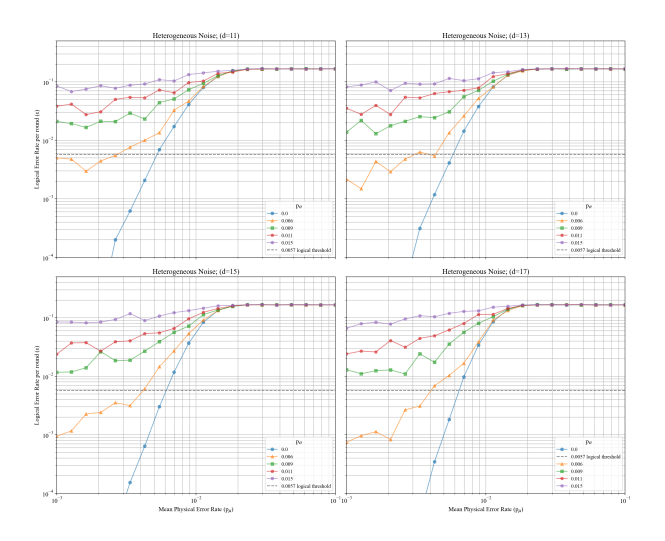


Fig. 12. (Case Study 3) Performance of heterogeneous noise model for distances 11 through 17. The blue line ( $p_{\sigma}$ = 0) represents a unilateral homogeneous noise model.

data qubit) and  $p_{def}$  range (from 0.05 to 0.75) is identical to the setup in Case 2 with the exception that the noise of all other qubits is distributed rather than uniform. For this experiment, we used the best performing deviation from Case 3 with a  $p_{\sigma}$ = 0.006 as the noise deviation value to use for all generated circuits. Interestingly, the performance trends shown in Case 4 (Fig. 14 and Fig. 15) follow a pattern similar to that observed in Case 2 (Fig. 7 and Fig. 8) in which increasing magnitudes of  $p_{def}$  result in relatively small deviations. However, the minimum viable code distance in this heterogeneous noise model is once again increased when compared to the minimum viable code distance with an identical defect setup in a homogeneous noise model in Case 2. For this heterogeneous model with a singular defect, the LER is not fully below the target  $\varepsilon_{thr}$  for all  $p_{def}$  until approximately d = 13 (Fig. 15). For d=9 (Fig. 14) and d=11

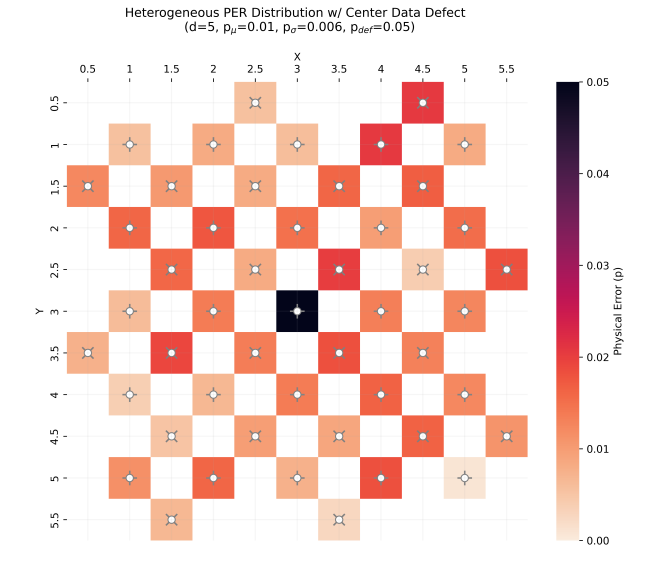


Fig. 13. (Case Study 4) Heatmap for a heterogeneous noise model on a d=5 code with an outlier center data qubit. In this heatmap, data qubits are denoted by + and measurement qubits are denoted with **X**.

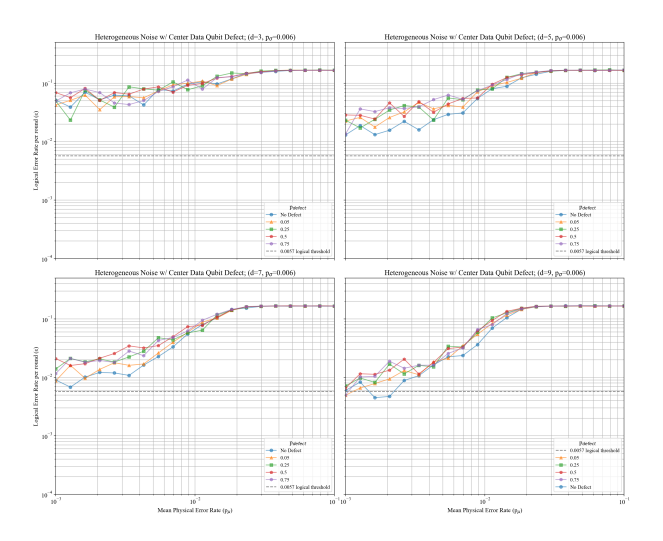


Fig. 14. (Case Study 4) Performance of heterogeneous noise model with center data defect for distances 3 through 9. In Case 4, we simulated the performance of a heterogeneous noise model with a singular center data qubit defect with  $p_{def}$  in the range of 0.05 to 0.75. The blue line represents a baseline heterogeneous noise model with no defects present. In all simulations in Case 4, the noise distribution has a deviation of  $p_{\sigma}$ =0.006. In the prior Case 3, the performance of  $p_{\sigma}$ =0.006 displayed the largest increase in performance when moving from low to high distance code and thus was chosen as the standard  $p_{\sigma}$  value to use when testing across increasing  $p_{def}$  values in Case 4.

(Fig. 15), the variations in the random distribution of noise cause too much inconsistency to concretely determine whether these distances would be sufficient to meet the target logical threshold.

## VI. DISCUSSION AND FUTURE WORK

Our experiments aimed to highlight how heterogeneity affects performance on the surface code, and the results indicate that the presumed model of noise greatly impacts the

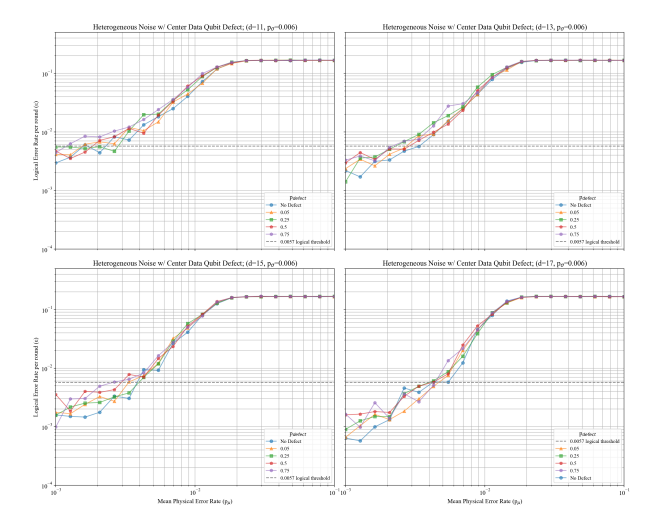


Fig. 15. (Case Study 4) Performance of heterogeneous noise model with center data defect for distances 11 through 17. The blue line represents a baseline heterogeneous noise model with no defects present.

purported performance of the surface code. We proposed in this work that, in order to accurately model surface code on superconducting qubits, accepting some level of heterogeneity is necessary due to the inherent nonuniform noise exhibited by superconducting qubits. The aim of our work is thus to provide a preliminary accounting of how the performance of heterogeneous distributions directly affects the LER. As shown in our experiments, the presence of a singular defective qubit with an error rate as high as 75% has a significantly less noticeable impact on our logical performance than the introduction of slightly deviated distributions in the fidelity of the qubit. One insight from these experiments is that, under both homogeneous and heterogeneous noise conditions, incredibly defective qubits have a surprisingly negligible effect on the LER.

In regards to the impacts of individual defects, the performance data for both a singular defect in the presence of heterogeneous and homogeneous noise models show that the defective qubit's impact is only non-negligible at distances at or closely above the minimum viable code distance (the distance at which the target LER is reachable).

In the performance experiments for Case 2 (Fig. 7 and Fig. 8), the minimum viable code distance occurs at d=5. At d=3, the target LER is not reachable even when there are no defects present. Although the performance at d=3 is insufficient, the performance across the increasing  $p_{def}$  noise is nearly identical, indicating that this defect has little impact on the LER. At d=5, the trend lines suddenly deviate, and the impact of higher  $p_{def}$  noise on performance is noticeable. At d=5 through d=9, this performance deviation between  $p_{def}$  noise begins to converge. At d=11 and above, the impact of an increasingly defective qubit is nearly negligible again. What we can extrapolate from this is that there exists a sort of "Goldilocks zone" in which the detrimental impact of increasing noise on the defective qubit is evident. Within

this "Goldilocks zone," choosing to drop out or mitigate the defective qubit with large  $p_{def}$  values could result in noticeable performance gains. At d=11 and above, however, the impact of this defective qubit, even at p=0.75, is negligible and thus implementing a mitigation technique incurs additional cost, such as an increase in physical overhead [29, 24] or circuit depth [5], but results in no performance gains. Ideally, when making design decisions, techniques that incur additional costs should only be used when there is a noticeable performance gain. In this way, our research suggests that treating defect mitigation should be viewed as an optimization problem in which we aim to only drop out qubits in which the resulting performance gain is non-negligible in light of the cost incurred by the mitigation method.

In Case 4, the same defect configuration (center data qubit) is tested with a heterogeneous noise model. In the performance experiments conducted (Fig. 14 and Fig. 15), the distribution of noise across the lattice is relatively small, with a standard deviation of  $p_{\sigma}$ = 0.006, but had a significant impact on the overall performance. At d=5 in Case 2, all lattices regardless of the defective qubits  $p_{def}$  value were able to meet the target LER threshold. However, with the introduction of heterogeneous noise in Case 4, a d=11 code is required for suppression of this defective qubit for all  $p_{def}$  values. Thus, these experiments suggest that even small noise deviations across a lattice have a far greater impact on performance than singular defective qubits with significant levels of noise.

In moving forward, we believe that the impacts of heterogeneity on surface code is vital as we continue to develop both physical devices and QEC techniques in order to reach faulttolerant quantum computing. Looking ahead, we believe there are many areas in which the work here could be expanded. A particular area of improvement would be to expand the simplified noise model that we use to create our circuits, such as introducing additional scaling factors to more accurately represent the different operational error rates [18]. Secondly, the experiments focused primarily on testing individual defects on a singular data qubit, but expanding these experiments to encompass how additional configurations of defect characteristics affect performance is an area for future work. Additionally, identifying how these defects accumulate would provide further insight into when deformation techniques are absolutely necessary. Overall, the experimental results presented in our research demonstrate preliminary evidence showing the existence of BADs as well as the disparity between viewing the surface code under a homogeneous model vs. a heterogeneous model. If the outcome of simulation is to optimize performance for computation on real devices, viewing the surface code in only a homogeneous regime results in vastly different design outcomes, such as picking optimal code distances to meet a target logical threshold.

#### VII. CONCLUSION

In this work, we explore the impact of heterogeneous noise on the performance of the SC. To the best of our knowledge, this work is among the first to study physical error rate of device qubits as a distribution rather than as a uniform mean. Using BADs, we explore the impact that both outlier qubits and normally-distributed physical errors have on SC LER. As a result of our work, we discovered that one bad qubit does not necessarily spoil the bunch, but instead, significant variation on-chip can have detrimental effects on logical fidelity. To conclude, this work motivates the inclusion of BADs in QEC analysis based on the SC, and we hope that the software framework developed by this work will open doors for design space exploration that creates shorter timelines between now and fault-tolerant quantum computing.

#### VIII. DECLARATIONS

#### A. Data Availability

The data and figures generated for this paper were created from our code and can be found on our GitHub repository at: https://github.com/JacobSPalmer/quantum-ddq-toolkit/tree/icrc-25. Additionally, all data used to generate the specific figures shown in the manuscript can be found here: https://github.com/JacobSPalmer/quantum-ddq-toolkit/tree/icrc-25/supplementary-materials.

#### B. Author Contributions

J. S. P. led code development and experiment implementations. K.N.S. advised project direction, and both authors contributed to the analysis and writing of the manuscript.

#### C. Funding

No funding was received in relation to this study. (Funding: Not Applicable)

# D. Competing Interests

The authors of this paper declare no competing interests.

#### REFERENCES

- [1] Rajeev Acharya et al. "Quantum error correction below the surface code threshold". en. In: *Nature* 638.8052 (Feb. 2025). Publisher: Nature Publishing Group, pp. 920–926. ISSN: 1476-4687. DOI: 10.1038/s41586-024-08449-y. URL: https://www.nature.com/articles/s41586-024-08449-y (visited on 09/28/2025).
- [2] James M Auger et al. "Fault-tolerance thresholds for the surface code with fabrication errors". In: *Physical Review A* 96.4 (2017), p. 042316.
- [3] James M. Auger et al. "Fault-tolerance thresholds for the surface code with fabrication errors". In: *Physical Review A* 96.4 (Oct. 2017). arXiv:1706.04912 [quant-ph], p. 042316. ISSN: 2469-9926, 2469-9934. DOI: 10. 1103/PhysRevA.96.042316. URL: http://arxiv.org/abs/1706.04912 (visited on 02/13/2025).
- [4] Samudra Dasgupta and Travis S Humble. "Reliable devices yield stable quantum computations". In: 2023 IEEE International Conference on Quantum Computing and Engineering (QCE). Vol. 2. IEEE. 2023, pp. 223–226.

- [5] Dripto M. Debroy et al. LUCI in the Surface Code with Dropouts. arXiv:2410.14891 [quant-ph]. Oct. 2024. DOI: 10.48550/arXiv.2410.14891. URL: http://arxiv. org/abs/2410.14891 (visited on 04/15/2025).
- [6] Eric Dennis et al. "Topological quantum memory". In: Journal of Mathematical Physics 43.9 (2002), pp. 4452– 4505.
- [7] Cirq Developers. *Cirq*. Zenodo. Aug. 2025. DOI: 10. 5281/ZENODO.16867504. (Visited on 10/06/2025).
- [8] Austin G Fowler et al. "Surface codes: Towards practical large-scale quantum computation". In: *Physical Review A—Atomic, Molecular, and Optical Physics* 86.3 (2012), p. 032324.
- [9] Austin G. Fowler et al. "Surface codes: Towards practical large-scale quantum computation". In: *Physical Review A* 86.3 (Sept. 2012). arXiv:1208.0928 [quant-ph], p. 032324. ISSN: 1050-2947, 1094-1622. DOI: 10. 1103/PhysRevA.86.032324. URL: http://arxiv.org/abs/1208.0928 (visited on 01/25/2025).
- [10] Craig Gidney. *Stim.* Version v1.15.0. May 2025. DOI: 10.5281/zenodo.15354872. URL: https://doi.org/10.5281/zenodo.15354872.
- [11] Craig Gidney. "Stim: a fast stabilizer circuit simulator". In: *Quantum* 5 (July 2021). arXiv:2103.02202 [quant-ph], p. 497. ISSN: 2521-327X. DOI: 10.22331/q-2021-07-06-497. URL: http://arxiv.org/abs/2103.02202 (visited on 10/05/2025).
- [12] Craig Gidney and Austin G. Fowler. "Efficient Magic State Factories with a Catalyzed \$—CCZ\rangle\$ to \$2—T\rangle\$ Transformation". In: *Quantum* 3 (Apr. 2019), p. 135. DOI: 10.22331/q-2019-04-30-135. (Visited on 10/07/2025).
- [13] Ali Javadi-Abhari et al. *Quantum Computing with Qiskit*. June 2024. DOI: 10.48550 / arXiv.2405.08810. arXiv: 2405.08810 [quant-ph]. (Visited on 10/06/2025).
- [14] Youngseok Kim et al. "Error Mitigation with Stabilized Noise in Superconducting Quantum Processors". In: *Nature Communications* 16.1 (Sept. 2025), p. 8439. ISSN: 2041-1723. DOI: 10.1038/s41467-025-62820-9. (Visited on 10/07/2025).
- [15] Sophia Fuhui Lin et al. "Codesign of quantum error-correcting codes and modular chiplets in the presence of defects". In: Proceedings of the 29th ACM International Conference on Architectural Support for Programming Languages and Operating Systems, Volume 2. arXiv:2305.00138 [quant-ph]. Apr. 2024, pp. 216–231. DOI: 10.1145/3620665.3640362. URL: http://arxiv.org/abs/2305.00138 (visited on 01/25/2025).
- [16] Daniel Litinski. "A game of surface codes: Large-scale quantum computing with lattice surgery". In: *Quantum* 3 (2019), p. 128.
- [17] Daniel Litinski. "Magic state distillation: Not as costly as you think". In: *Quantum* 3 (2019), p. 205.
- [18] Masoud Mohseni et al. How to Build a Quantum Supercomputer: Scaling from Hundreds to Millions of

- *Qubits.* arXiv:2411.10406 [quant-ph]. Jan. 2025. DOI: 10.48550/arXiv.2411.10406. URL: http://arxiv.org/abs/2411.10406 (visited on 10/02/2025).
- [19] Masoud Mohseni et al. "How to build a quantum supercomputer: Scaling from hundreds to millions of qubits". In: *arXiv preprint arXiv:2411.10406* (2024).
- [20] Prakash Murali et al. "Noise-adaptive compiler mappings for noisy intermediate-scale quantum computers". In: *Proceedings of the twenty-fourth international conference on architectural support for programming languages and operating systems*. 2019, pp. 1015–1029.
- [21] Michael Nielsen and Isaac L. Chuang. Quantum Quantum Computation and Information: 10th Anniversary Edition. https://www.cambridge.org/highereducation/books/quantumcomputation-and-quantuminformation/01E10196D0A682A6AEFFEA52D53BE9AE. Dec. 2010. DOI: 10.1017/CBO9780511976667. (Visited on 10/06/2025).
- [22] "Quantum error correction below the surface code threshold". In: *Nature* 638.8052 (2025), pp. 920–926.
- [23] Salonik Resch and Ulya R. Karpuzcu. "Benchmarking Quantum Computers and the Impact of Quantum Noise". In: ACM Comput. Surv. 54.7 (July 2021), 142:1–142:35. ISSN: 0360-0300. DOI: 10. 1145 / 3464420. URL: https://dl.acm.org/doi/10.1145/3464420 (visited on 09/27/2025).
- [24] Kaitlin N Smith et al. "Scaling superconducting quantum computers with chiplet architectures". In: 2022 55th IEEE/ACM International Symposium on Microarchitecture (MICRO). IEEE. 2022, pp. 1092–1109.
- [25] Armands Strikis, Simon C Benjamin, and Benjamin J Brown. "Quantum computing is scalable on a planar array of qubits with fabrication defects". In: *Physical Review Applied* 19.6 (2023), p. 064081.
- [26] Youngkyu Sung et al. "Non-Gaussian Noise Spectroscopy with a Superconducting Qubit Sensor". In: *Nature Communications* 10.1 (Sept. 2019), p. 3715. ISSN: 2041-1723. DOI: 10.1038/s41467-019-11699-4. (Visited on 10/06/2025).
- [27] Swamit S Tannu and Moinuddin K Qureshi. "Not all qubits are created equal: A case for variability-aware policies for NISQ-era quantum computers". In: *Proceedings of the twenty-fourth international conference on architectural support for programming languages and operating systems*. 2019, pp. 987–999.
- [28] Yu Tomita and Krysta M. Svore. "Low-Distance Surface Codes under Realistic Quantum Noise". In: *Physical Review A* 90.6 (Dec. 2014), p. 062320. ISSN: 1050-2947, 1094-1622. DOI: 10.1103 / PhysRevA. 90. 062320. arXiv: 1404.3747 [quant-ph]. (Visited on 10/06/2025).
- [29] Keyi Yin et al. Surf-Deformer: Mitigating Dynamic Defects on Surface Code via Adaptive Deformation. arXiv:2405.06941 [quant-ph]. Sept. 2024. DOI: 10.

48550/arXiv.2405.06941. URL: http://arxiv.org/abs/2405.06941 (visited on 05/06/2025).